SANDIA REPORT

SAND2005-0101
Unlimited Release
Printed July 2001

GeSi Strained Nanostructure Self-Assembly for Nano- and Opto-Electronics

Jerrold A. Floro and Joel L. Means

Prepared by
Sandia National Laboratories
Albuquerque, New Mexico 87185 and Livermore, California 94550

Sandia is a multiprogram laboratory operated by Sandia Corporation,
a Lockheed Martin Company, for the United States Department of Energy's
National Nuclear Security Administration under Contract DE-AC04-94AL85000.

Approved for public release; further dissemination unlimited.

Issued by Sandia National Laboratories, operated for the United States Department of Energy by Sandia Corporation.

NOTICE: This report was prepared as an account of work sponsored by an agency of the United States Government. Neither the United States Government, nor any agency thereof, nor any of their employees, nor any of their contractors, subcontractors, or their employees, make any warranty, express or implied, or assume any legal liability or responsibility for the accuracy, completeness, or usefulness of any information, apparatus, product, or process disclosed, or represent that its use would not infringe privately owned rights. Reference herein to any specific commercial product, process, or service by trade name, trademark, manufacturer, or otherwise, does not necessarily constitute or imply its endorsement, recommendation, or favoring by the United States Government, any agency thereof, or any of their contractors or subcontractors. The views and opinions expressed herein do not necessarily state or reflect those of the United States Government, any agency thereof, or any of their contractors.

Printed in the United States of America. This report has been reproduced directly from the best available copy.

Available to DOE and DOE contractors from
U.S. Department of Energy
Office of Scientific and Technical Information
P.O. Box 62
Oak Ridge, TN 37831

Telephone: (865)576-8401
Facsimile: (865)576-5728
E-Mail: reports@adonis.osti.gov
Online ordering: http://www.osti.gov/bridge

Available to the public from
U.S. Department of Commerce
National Technical Information Service
5285 Port Royal Rd
Springfield, VA 22161

Telephone: (800)553-6847
Facsimile: (703)605-6900
E-Mail: orders@ntis.fedworld.gov
Online order: http://www.ntis.gov/help/ordermethods.asp?loc=7-4-0#online

SAND2005-0101
Unlimited Release
Printed July 2001

GeSi Strained Nanostructure Self-Assembly for Nano- and Opto-Electronics

Jerrold A. Floro
Surface and Interface Sciences Department
Sandia National Laboratories
P. O. Box 5800
Albuquerque, NM 87185-1415

Joel L. Means
Department of Physics
Texas A&M University
College Station, TX 77843

ABSTRACT

Strain-induced self-assembly during semiconductor heteroepitaxy offers a promising approach to produce quantum nanostructures for nanologic and optoelectronics applications. Our current research direction aims to move beyond self-assembly of the basic quantum dot towards the fabrication of more complex, potentially functional structures such as quantum dot molecules and quantum wires. This report summarizes the steps taken to improve the growth quality of our GeSi molecular beam epitaxy process, and then highlights the outcomes of this effort. *This is the final report for LDRD 79943, "GeSi Strained Nanostructure Self-Assembly for Nano- and Opto-Electronics"*.

Intentionally Left Blank

Contents

Introduction ……………………………………………………………………………………6
Background ………………………………………………………………..………………...6
Experimental Techniques ……………..…………………………………..…………………..8
Growth Degradation ………………..……………………………………..…………………..8
Project Results and Accomplishments ……………..……………………..…………………..9
Results of the contamination control study ……….….…………………………………....9
Source contamination ………………………………………………………………………9
Wafer cleaning ….…..………………………………………………………………………9
Substrate plate contamination ………………………………………………………………9
Si buffer thickness.………………………………………………………………………10
Limiting time from buffer to alloy.…………………………………………………………10
Alloy growth temperature.…………………………………………………………………10
MBE base pressure.………………………………………………………………………...10
Reduction of buffer growth temperature.….………………………………………………10
Important post-contamination accomplishments ..……………….…………………………11
Pit characterization ……..…………………………………………………………………12
Directed self-assembly.……………….……………………………………………………13
Summary of findings ………………...………………………………..…………………...13
References………………………………………………………………………………..15

Figures

1 Scanning electron micrograph of {105} pyramidal quantum dots …………………………..6
2 AFM topographs of $Ge_{0.3}Si_{0.7}$ films grown at 550°C, 0.09 nm/s ..…………………….……..7
3 AFM topograph, 3x3 µm, showing morphology of a $Ge_{0.3}Si_{0.7}$ film, 20 nm thick, under contaminated conditions ………………………………………………………………………....9
4 AFM topograph, 5x5 µm, of QDMs formed after switching to a lower temperature process …………………………………………………………………………………………….....11
5 AFM topographs, 1.3x1.3 µm, showing the evolution of pits formed after switching to a lower temperature process …………………………………………………………………....12
6 Line profiles from pits in the images of Figure 5. …………………………………………13
7 Scanning electron micrographs showing aligned QDMs on holes created in the original Si wafer using a focused ion beam. ………………………………………………………..…….. 14

Introduction

In a coherently strained, heteroepitaxial thin film, the stored elastic energy can do work upon the film, either in the form of shear, mediated by the passage of misfit dislocation half-loops, or in the form of three dimensional roughening, mediated by the surface mass transport of adatoms. The latter mechanism can be exploited to self-assemble quantum nanostructures, e.g., dots and wires that might be useful in high-performance optoelectronics, nanologic, or low-dimensional physics studies.

Strain-induced quantum dot formation is considered to be a limited form of self-assembly – dots form "on their own", but they typically lack many requisite characteristics to be fully useful. Ideally, complete self-assembly would result in dots with the desired size, shape, composition (or strain), isolation, and placement in order to form a functional array for a desired application. We are still far from achieving this, but steady progress is being made in controlling and understanding many important aspects of strain-induced heteroepitaxial self-assembly.

Our work examines how deposition parameters can be manipulated to form bound assemblages of quantum dots, i.e., quantum dot molecules (QDMs), during molecular beam epitaxial growth of $Ge_{0.3}$ $Si_{0.7}$ films on Si (001) substrates. QDMs form in a growth regime where *pit* formation, rather than islanding, occurs as the initial means of strain relief during heteroepitaxy.

Background

When Ge_xSi_{1-x} (x=0.2-0.3) alloy films are grown at 750°C and 0.01 nm/s, the surface morphological evolution follows the well-established sequence of (1) planar wetting layer growth for 1.5-2.5 nm, (2) 3D roughening via a strain-driven instability [1,2], (3) formation of {105} faceted, pyramidal quantum dots from the initial instability, [3-6], (4) ordering and ripening of the pyramid array [7,8], (5) transition to dome clusters when pyramids exceed their critical volume, as shown in Fig. 1 [9-12], and (6) misfit dislocation formation, possibly accompanied by superdome formation [5,11]. A similar transition sequence is observed with increasing Ge fraction in the alloy up to pure Ge, but the relevant length scales are reduced, and lower deposition temperatures can be used in order to observe the sequence [5].

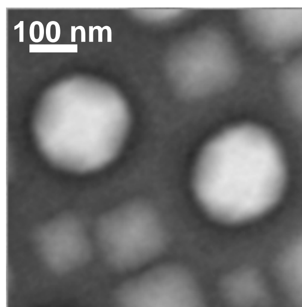

Figure 1. Scanning electron micrograph of {105} pyramidal quantum dots (the islands with square bases) and domes (the two larger, more rounded islands). The film is $Ge_{0.3}Si_{0.7}$/Si (001), 6 nm thick, and grown at 750°C.

However, when $Ge_{0.3}Si_{0.7}$ / Si(001) films are grown at 550°C and 0.09 nm/s, the morphological evolution is quite different [13]. Under these more limited growth kinetics, the film is constrained to grow a metastable wetting layer up to a film thickness of 5 nm. Now, the first 3D roughening that occurs is in the form of *pits* in the metastable wetting layer, rather than islands, as shown in the atomic force microscope topographic image (AFM) of Fig. 2(a). With further deposition, the pits enlarge and the material

ejected from the pits accumulates alongside to form four quantum dots (Fig. 2(b)), in a "cooperative nucleation" process described by Jesson et al. [14]. As deposition proceeds, the 4-fold symmetric "quantum dot molecules" form {105} faceted pits (Fig. 2(c)) and the separate islands eventually join together to form a continuous wall surrounding the pit, a structure we variously have referred to as the quantum fortress or mature QDM, as shown in Fig. 3(d).

QDMs are an example of higher-order self-assembly — in a sense, four nanostructures are

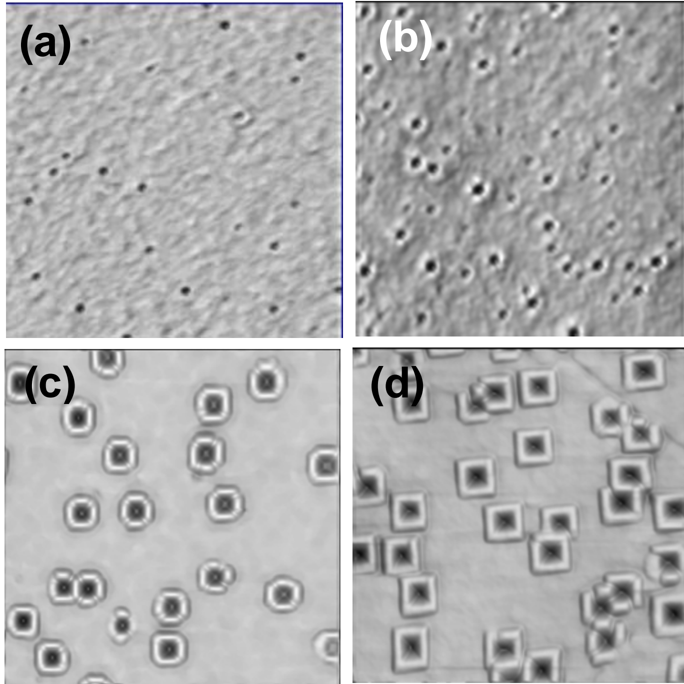

Figure 2. AFM topographs of $Ge_{0.3}Si_{0.7}$ films grown at 550°C, 0.09 nm/s on Si (001), as a function of mass equivalent film thickess. Thicknesses are (a) 5 nm, (b) 15 nm, (c) 20 nm, and (d) 30 nm.

obtained for the price of one. Four-fold QDMs are of interest in the nanologic architecture known as Quantum Cellular Automata (QCA). A basic QCA cell is comprised of four proximal quantum dots, two of which contain electronic charge [14]. The charges occupy opposite corners due to repulsion, but the state is bi-stable (i.e., the charges could also occupy the other two corners) if the structure is symmetric and the dots are spaced such that tunneling can occur. By aligning a series of QCA cells in a specific geometric pattern, logic gates can be fabricated that contain no internal wiring – all the switching is via electrostatic interactions and tunneling. QCA offers nominal simplicity, low power operation, and compactness, making it potentially attractive for next generation logic, although very significant hurdles remain to be surmounted.

Because QDM formation is a kinetically controlled self-assembly process that occurs in a fairly narrow window of MBE process-parameter space, it is important to have good control over the process variables such as deposition temperature and rate. Furthermore, the areal density, faceting, and symmetry of QDMs are extremely sensitive to contamination that can arise from multiple points in the process flow. The primary goal of the LDRD was to investigate in more detail the origins of pit formation by characterizing the evolution of pit morphology. However, as we will discuss below, an unknown source of contamination crept into our process in mid/late 2003 that progressively worsened, requiring a concerted effort to solve in order to make further progress on QDM formation.

EXPERIMENTAL TECHNIQUES

Our GeSi alloy films were grown using electron beam co-evaporation in a custom-design molecular beam epitaxy (MBE) chamber at Sandia. Evaporation sources were 40cc monolithic starter sources with 99.999% initial purity. The base pressure of the chamber is at or below $1x10^{-10}$ Torr, but the pressure rises to $1\text{-}2x10^{-8}$ Torr during deposition, primarily due to hydrogen, but also with some (less than $1x10^{-9}$ Torr partial pressure) CO, CO_2, and CH_4 from the hot filaments. Partial pressures of O_2 and H_2O remain at or below $1x10^{-10}$ Torr. Deposition rates are measured and controlled using calibrated quartz crystal oscillators. All heating is by radiative transfer from a nude W filament. The sample temperature is monitored using a pyrometer, but absolute temperature is only known to within about 25^oC.

The substrates are diced from undoped Si (001) wafers from Virginia Semiconductor, with a miscut no greater than 0.1^o. The sample dimensions are 0.5" x 1.5" x 0.012" thick. Cleaning for epitaxy involves chemical formation of a non-stoichiometric oxide that is ultimately removed by in situ desorption just before buffer growth. All chemicals are clean-room electronic grade (Ashland Megabit or LP grades), and the rinse water is flowing, ultrafiltered 18 MW deionized water. After dicing, the substrates are first subjected to solvent degreasing, both in ultrasonic (2-propanol and acetone) and at elevated temperatures (trichloroethylene at 80^oC). The next step is removal of residual hydrocarbons using a 4:1 H_2SO_4:H_2O_2 mixture that is exothermically heated. Trace transition metals are removed using the sequence: etch in 1:1:4 HCl:H_2O_2:H_2O at 80^oC, rinse, oxide removal in 7:1 buffered oxide etch, which is repeated three times. The chemical oxide is formed using a 3:1:1 HCl:H_2O_2:H_2O solution at 80^oC, followed by an extensive rinse, N_2 blow dry, after which the sample is immediately mounted to a Mo platen and pumped down in the MBE load lock.

After transfer into the growth chamber, samples are degassed by ramping from room temperature to 630^oC over 14-20 hours. Oxide desorption occurs during 820^oC annealing for 15 minutes, with continuous monitoring of the surface structure using reflection high-energy electron diffraction (RHEED). A Si buffer layer is then grown 100 nm thick at 750^oC, using a low/high/low sequence for the deposition rate. The typical RHEED pattern after buffer growth consists of a Laue circle of intense spots at both integral and half-order positions, characteristic of a smooth, 2x1 reconstructed surface.

GROWTH DEGRADATION

The structures shown in Figure 2 were mostly grown in the timeframe 2001-2003. In the last year and a half we have had increasing difficulty obtaining these structures with a quality sufficient to allow further study and morphological tailoring. Figure 3 shows an example of recent poor results. There are two observed structures that we empirically associate with impurity effects: (1) macropits that extend through both the alloy and the buffer, which are immersed within a dense matrix of QDMs, and (2) a high density of small features forming extended rough patches, in which QDMs cannot form. Although the original intent of the LDRD

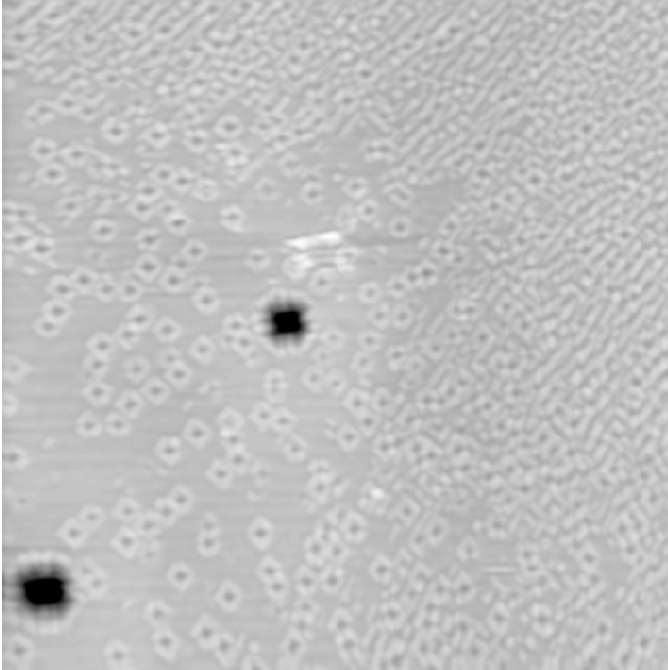

Figure 3. AFM topograph, 3x3 mm, showing morphology of a Ge0.3Si0.7 film, 20 nm thick, under contaminated conditions. Two macropits are observed in a field of QDMs, as well as an extended area of very high density ridges and QDMs.

was not to investigate and control contamination, this route was forced upon us in order to make any subsequent scientific or technical progress.

PROJECT RESULTS AND ACCOMPLISHMENTS

Results of the contamination control study

Most of the work of this LDRD, which took place over the summer of 2004, was focused on solving contamination problems so that we could proceed with work on understanding the origins of pit formation and on tailoring the location and alignment of QDMs. A number of issues were investigated, as discussed below, before the problem was ultimately solved.

Source contamination: The alloy films are deposited by e-beam evaporation from ultra-high-purity solid sources. Contamination of the sources with Ni can occur, since the water-cooled e-beam pockets these sources reside in are Ni-lined. Both the Si and Ge sources were replaced with brand new starter sources, but this did not fix the problem.

Wafer cleaning: The Si substrates were subjected to an extensive wet cleaning process as described above. We examined the process deionized water, the chemical purity of acids and solvents, the cleanliness of the hood environment and the beakers and tweezers. None of this had a noticeable effect.

Substrate plate contamination: The Si substrates were strip-shaped pieces that were mounted in a molybdenum “picture frame” holder. We replaced some of the tooling on the holder, and ultimately began using full two-inch wafers without the Mo holder at all, but these trials did not solve the problem.

Si buffer thickness: Some of our earlier results seemed to suggest that problems with the Si buffer increased as a function of its thickness, so we investigated how reduction of the buffer thickness might improve quality of the subsequent alloy growth. However, systematic variation of the buffer identified no consistent trend and was not a solution.

Limiting time from buffer to alloy: After the clean Si buffer is grown, there is typically a period of 60-90 minutes in which the sample is cooled from 750°C, where the buffer is grown, to 550°C for alloy deposition. During this time, impurities from the background gas are impinging on the clean sample, and some fraction could adsorb. We cut down the time between buffer and alloy by factors of up to three, without positive effect.

Alloy growth temperature: From past work we know that the formation of QDMs can be quite sensitive to the substrate temperature. In particular, if the substrate is only 10-20° too warm, the film can destabilize to form extended 3D roughness that supercedes QDM formation, somewhat similar to what is seen in Fig. 3. We systematically varied the deposition temperature about the nominal ideal temperature, but without finding any consistent improvement in growth quality.

MBE base pressure: The MBE chamber has, over the years, consistently reached base pressures of less than $1x10^{-10}$ Torr once it is well-baked and conditioned by a series of growths. In about the same time span that growth quality declined we have noted some degradation in the vacuum performance as well, where base pressures would not consistently enter the 10^{-11} Torr regime. During the summer, after the system was vented for cleaning and cryopump modification, we performed an extensive bakeout (8 days at approximately 150°C instead of the typical 5 days), and we tried an additional treatment – exposure of the hot chamber to molecular hydrogen in the $1x10^{-6}$ Torr range for the last 24 hours of bakeout. There was significant improvement in vacuum performance, with the chamber pressure dropping below $4x10^{-11}$ Torr over a one-month period – performance similar to or better than historically achieved. This is attributed primarily to the introduction of hydrogen during the bake, although we did not perform a control experiment where we independently changed bake time and hydrogen exposure. The decrease background pressure did reduce the density of 3D features during GeSi alloy growth, which is desirable, but did not totally eliminate macropit formation.

Reduction of buffer growth temperature: During our investigations using full two-inch diameter wafers, which have a temperature variation of about -25°C at the wafer edge for a center temperature of 815°C, we noted that good quality structures were obtained in the cooler region near the edge, with no macropits whatsoever. This was a key observation, but was subject to two interpretations: were cooler temperatures during alloy growth or during buffer growth most important? Since we had already examined the effect of reducing the alloy growth temperature, without positive effect, we then turned to reducing the buffer temperature. In particular, the first 30 Å of the buffer was being grown at 0.05 Å/s and 815-820°C (the temperature used to desorb the non-stoichiometric oxide), then the buffer was cooled down to 750°C for the rest of the growth. We decided to examine the effect of limiting the maximum process temperature to 750°C, including the oxide desorption step. This necessitated changing the desorption to a Si beam-assisted process, wherein a flux of Si of less than 0.1 Å/s effective rate is employed to help destabilize the chemical oxide and enhance the desorption rate. This

process resulting in the growth of smooth buffers (according to in situ RHEED) and, more importantly, completely eliminated macropit formation and other unwanted roughening during alloy growth. Combined with the cleaner chamber using the H_2-assisted bakeout, we were able to begin growing quantum dot molecule arrays that were symmetric, highly faceted, and of very low areal density. These characteristics were as good or better than ever achieved previously.

Although the contamination problem was ultimately solved, we do not fully understand the solution! The high temperature step that seems to be the source of the problems has been in use for at least three years, so it is not clear what changed in the last year or so. The nature of the contaminant itself is also not known definitively. Carbon on the Si surface can form carbide precipitates and subsequent silicon buffer growth will tend to avoid overgrowing these precipitates due to the large lattice and chemical mismatch [15]. It is possible that the sample manipulator/heater, which was removed and repaired early in 2004, became somewhat contaminated (especially the new heater filament), and that this created an increased local impurity "atmosphere" when the heater assembly was driven hard to obtain sample temperatures of 820°C. Depth profiling to assay impurity content in the film was attempted using secondary ion mass spectroscopy (SIMS). Unfortunately, only a surface profile was obtained (that was inconclusive due to oxidation); depth profiling was thwarted by sample charging effects.

Important post-contamination accomplishments

Figure 4 shows a typical array of GeSi QDMs achieved using the modified Si buffer growth process. The low areal density and high degree of symmetry provides confidence in the overall growth process. We then proceeded with two key experiments – a study of pit shapes, and growth of QDMs on patterned Si wafers (aspects of this work are co-funded by our BES Advanced Growth project). Preliminary results are briefly described below.

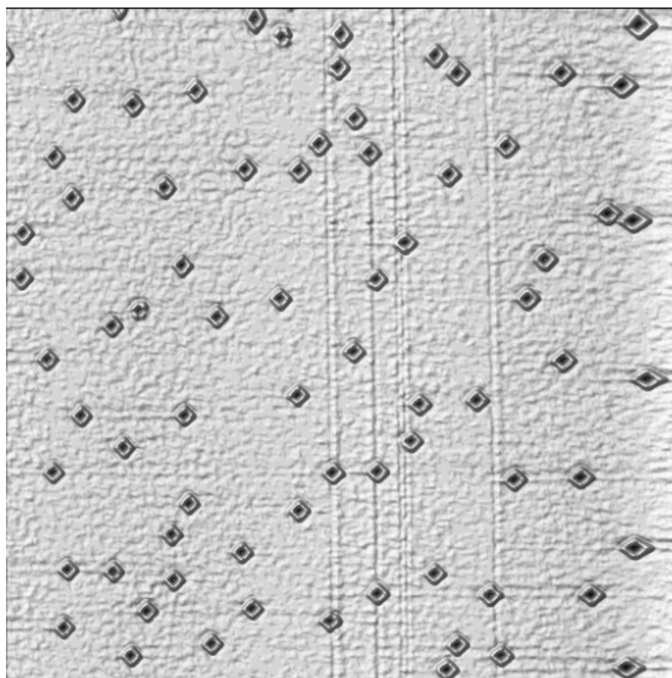

Figure 4. AFM topograph, 5x5 μm, of QDMs formed after switching to a lower temperature process for chemical oxide desorption and buffer layer growth, and improving the chamber base vacuum. The areal density of QDMs is about 3 μm^{-1}, which is quite low, and the shape and symmetry of the structures is quite good.

Pit characterization: The key mechanism leading to QDM self-assembly is the preferential formation of pits rather than islands as the preferred 3D roughening/strain relaxation mechanism under kinetically controlled conditions where adatom mobility is limited (but not vanishing). However, we do not understand in detail how pits form. The basic question is whether pits arise via nucleation [16] or via an instability [17]. Nucleation seems an obvious choice – pits are localized structures with separation that are large compared with the lateral dimensions of the pits. Instabilities, on the other hand, are barrierless, delocalized roughening transitions producing wavelike structures on the surface that ultimately become island-like when the troughs of the waves reach the substrate surface. True nucleation requires that the pits be faceted, so we have endeavored to grow pits and perform ex situ atomic force microscopy (AFM) to characterize the shape of the pits.

Figure 5 shows surface morphology of films grown to 7.2, 8.4 and 10.2 nm mass equivalent film thickness. While pits were clearly forming at 5 nm in our earlier studies, no pits are observed at 5 nm in the recent studies in the cleaner chamber using the reduced temperature desorb/buffer process. Pit formation begins at about 7 nm, but the density of pits is lower than observed previously. These results suggest that impurities likely play some role in the formation of pits, as we see fewer pits, and later development of pits, when the base pressure of the MBE is improved.

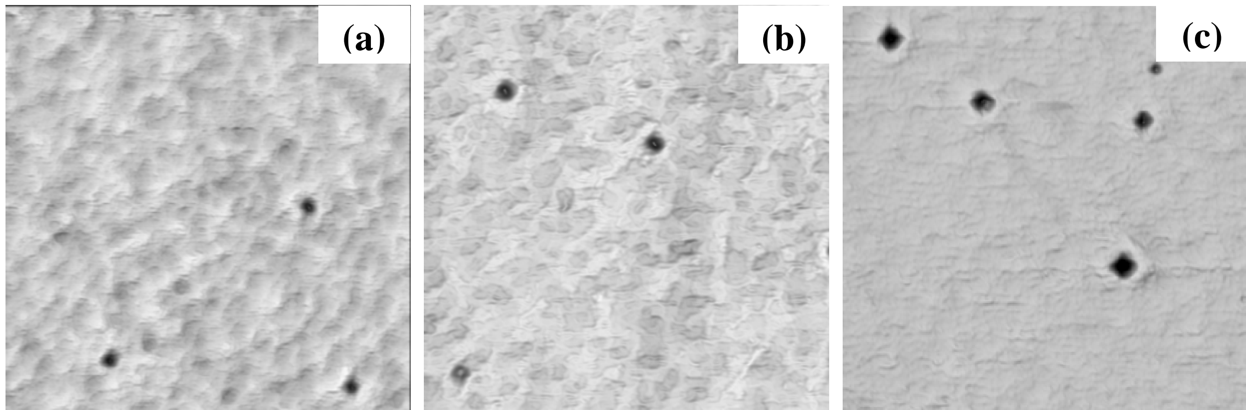

Figure 5. AFM topographs, 1.3x1.3 μm, showing the evolution of pits formed after switching to a lower temperature process for chemical oxide desorption and buffer layer growth, and improving the chamber base vacuum. Film thickness is (a) 72 Å, (b) 84 Å, and (c) 102 Å.

Figure 6 shows AFM linescans of three differently sized pits, where the shape progression is apparent. Faceting is not clearly observed. Although this is subject to concerns about AFM resolution and tip convolution effects, we have not observed facets in any of the early-stage pits we have examined, which rules against a nucleation mechanism.

We recently used 2D kinetic Monte Carlo calculations to show that pit formation can be observed in simulations that capture many aspects of strain-layer epitaxial growth. The simulations suggest a “damped instability” that effectively produces a localized pit, but without

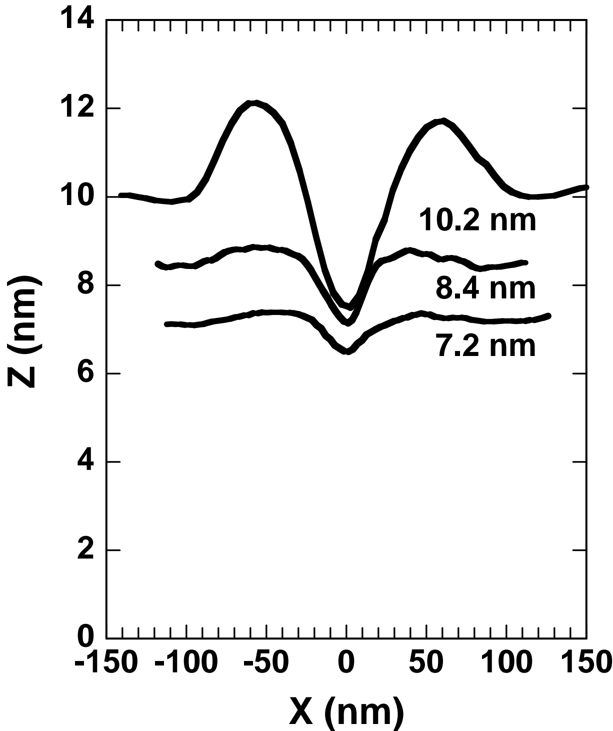

Figure 6. Line profiles from pits in the images of Figure 5. The profiles have been offset vertically to reflect the corresponding mass equivalent film thickness, as labeled (that is, the bottom axis represents the location of the film/buffer heterointerface).

faceting. Our results seem to support this, with the proviso that impurities may help dictate where the instability first develops.

Directed self-assembly: We used a focused ion beam to create periodic arrays of nanoscale holes in a Si substrate, and then, after the usual cleaning procedure, grew GeSi films on the patterned wafer. Figure 7 shows the exciting results: QDMs are precisely aligned on the patterned wafers, and when the pattern spacing is small enough, random QDMs are minimal. These results suggest a route towards directed self-assembly of QCA logic that we will continue to vigorously pursue.

Summary of findings

Through exhaustive iteration on a variety of process parameters associated with molecular beam epitaxial growth of GeSi alloys on Si (001), we significantly improved the growth conditions relevant to formation of high quality arrays of quantum dot molecules. The key factors driving the improvement were: (1) reduction of process temperature during chemical oxide desorption, and (2) improvement of chamber vacuum using an extended bake coupled with exposure to molecular hydrogen.

As a result of the improved process conditions, we are now able to proceed with detailed characterization of pit evolution, which is the critical step in formation of quantum dot molecules. Additionally, we obtained a definitive proof-of-principle that QDMs can be precisely positioned using ex situ patterns of holes generated in the Si substrate by a focused ion beam.

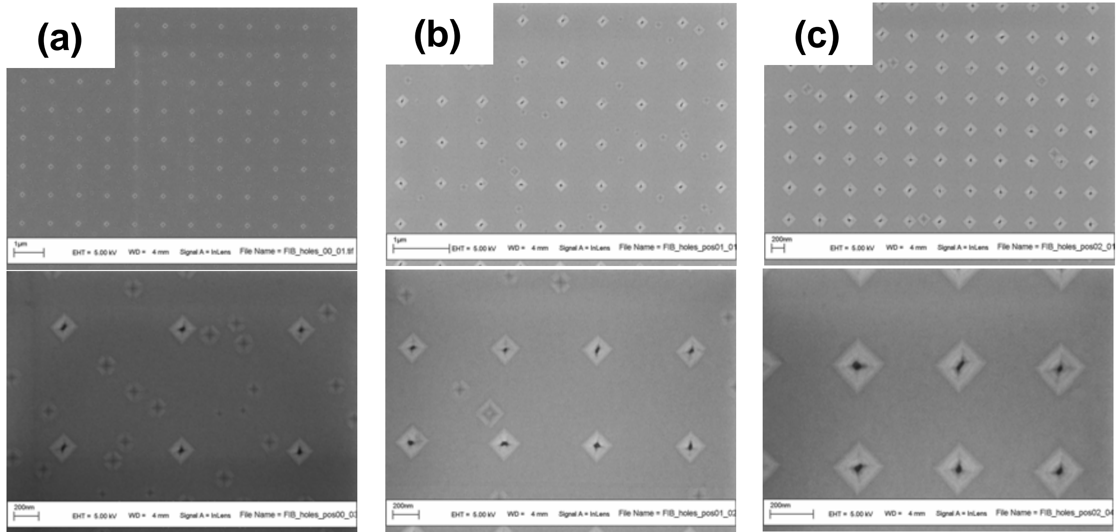

Figure 7. Scanning electron micrographs showing aligned QDMs on holes created in the original Si wafer using a focused ion beam. Spacings of the patterned holes are: (a) 1 μm, (b) 0.75 μm, and (c) 0.5 μm.

References

1. R. M. Tromp, F. M. Ross, M. C. Reuter, Phys. Rev. Lett. **84**, 4641 (2000).
2. P. Sutter, M. G. Lagally, Phys. Rev. Lett. **84**, 4637 (2000).
3. Y.-W. Mo, D. E. Savage, B. S. Swartzentruber, and M. G. Lagally, Phys. Rev. Lett. **65**, 1020 (1990).
4. J. A. Floro, E. Chason, R. D. Twesten, R. Q. Hwang, and L. B. Freund, Phys. Rev. Lett. **79**, 3946 (1997).
5. J. A. Floro, E. Chason, L. B. Freund, R. D. Twesten, and R. Q. Hwang, Phys. Rev. B **59**, 1990 (1999).
6. A. Rastelli and H. von Kanel, Surf. Sci. **532**, 769 (2003).
7. J. A. Floro, M. B. Sinclair, E. Chason, L. B. Freund, R. D. Twesten, R. Q. Hwang, and G. A. Lucadamo, Phys. Rev. Lett. **84**, 701 (2000).
8. J. A. Floro, E. Chason, M. Sinclair, L. B. Freund, and G. A. Lucadamo, Appl. Phys. Lett. **73**, 951 (1998).
9. M. Tomitori, K. Watanabe, M. Kobayashi, and O. Nishikawa, Appl. Surf. Sci. **76/77**, 322 (1994).
10. F. M. Ross, J. Tersoff, and R. M. Tromp, Phys. Rev. Lett. **80**, 984 (1998).
11. Gilberto Medeiros-Ribeiro, Alexander M. Bratkovski, Theodore I. Kamins, Douglas A. A. Ohlberg, and R. Stanley Williams, Science **279**, 353 (1998).
12. J. A. Floro, G. A. Lucadamo, E. Chason, L. B. Freund, M. Sinclair, R. D. Twesten, and R. Q. Hwang, Phys. Rev. Lett. **80**, 4717 (1998).
13. Jennifer L. Gray, Robert Hull, and Jerrold A. Floro, Appl. Phys. Lett. **81**, 2445 (2002).
14. G. Bernstein, C. Bazan, M. Chen, C. S. Lent, J. L. Merz, A. O. Orlov, W. Porod, G. L. Snider, and P. D. Tougaw, Superlattices and Microstructures **20**, 447 (1996).
15. X. Deng and M. Krishnamurthy, Phys. Rev. Lett. **81**, 1473 (1998).
16. J. Tersoff and F. Le Goues, Phys. Rev. Lett. **72**, 3570 (1994).
17. J. Tersoff, B.J. Spencer, A. Rastelli, and H. von Känel, Phys. Rev. Lett. **89**, 196104 (2002).

Distribution

1		Joel Means Department of Physics Mail Stop 4242 Texas A&M University College Station, TX 77843
1	MS 0123	Donna Chavez, LDRD Office, 1011
1	MS 0724	Les Shephard, 6000
2	MS 0899	Technical Library, 9616
1	MS 1033	Joe Tillerson, 6216
5	MS 1415	Jerrold A. Floro, 1114
1	MS 1427	Julia M. Phillips, 1100
1	MS 1415	Neal D. Shinn, 1114
1	MS 9018	Central Technical Files, 8945-1